Inorganics **2015**, *3*, 374-387; doi:10.3390/inorganics3030374

OPEN ACCESS

inorganics

ISSN 2304-6740

www.mdpi.com/journal/inorganics

Article

Water Oxidation by Ru-Polyoxometalate Catalysts: Overpotential Dependency on the Number and Charge of the Metal Centers

Simone Piccinin* and Stefano Fabris

CNR-IOM DEMOCRITOS, Istituto Officina dei Materiali, c/o SISSA, Via Bonomea 265, Trieste 34136, Italy; E-Mail: fabris@democritos.it

* Author to whom correspondence should be addressed; E-Mail: piccinin@iom.cnr.it; Tel: +39-40-3787317.

Academic Editors: Greta Ricarda Patzke and Pierre-Emmanuel Car

Received: 15 April 2015 / Accepted: 3 July 2015 / Published: 2 September 2015

Abstract: Water oxidation is efficiently catalyzed by several Ru-based polyoxometalate (POM) molecular catalysts differing in the number, local atomistic environment and oxidation state of the Ru sites. We employ density functional theory calculations to rationalize the dependency of the reaction overpotential on the main structural and electronic molecular properties. In particular, we compare the thermodynamics of the water oxidation cycle for single-site Ru-POM and multiple-site Ru_4-POM complexes. For the Ru-POM case, we also investigate the reaction free energy as a function of the Ru oxidation state. We find that the overpotential of these molecular catalysts is primarily determined by the oxidation state of the metal center and is minimum for Ru(IV). In solution, the number of active sites is shown to play a minor role on the reaction energetics. The results are rationalized and discussed in terms of the local structure around the active sites and of the electrostatic screening due to the molecular structure or the solvent.

Keywords: water oxidation; DFT; polyoxometalates; electrochemistry

1. Introduction

Replacing fossil fuels with renewable energy sources, like solar and wind, requires developing a strategy to cope with the intrinsic variability of these sources. To this end, Nature employs photosynthesis, which enables plants to convert sunlight into chemical energy through electrochemical reactions where H_2O and CO_2 are the reactants, while sugars and O_2 are the products. Mimicking this process with artificial devices would allow storing solar energy in the form of chemical fuels, which can be used at a later time to generate heat or electricity through combustion or fuel cells. Developing these technologies with high-enough efficiency is one of the current grand challenges in physical sciences [1,2].

One of the main bottlenecks for artificial solar fuel production is the lack of efficient, stable and inexpensive catalytic materials for the anodic reaction, the oxidation of water:

$$2H_2O \rightarrow O_2 + 4H^+ + 4e^- \quad (1)$$

The oxidation potential of this four-electron semi-reaction is 1.23 V, measured at pH = 0 against the normal hydrogen electron (NHE). This high oxidation potential reflects the high stability of water:

$$\Delta G^0(2H_2O \rightarrow O_2 + 4H_2) = 4.92\ \text{eV} \quad (2)$$

Using sunlight to promote the electrochemical splitting of water would therefore afford storing solar energy in the rearrangement of the chemical bonds among hydrogen and oxygen atoms, producing molecular H_2. Using the electrons released to the anode through the oxidation of water to reduce CO_2, rather than protons, would lead to the production of more manageable fuels, like, for example, methanol. Regardless of the fuel produced at the cathode, the source of electrons and protons at the cathode will be water, and suitable catalysts are needed to facilitate its oxidation.

RuO_2 and IrO_2 catalysts, although efficient, suffer from poor stability in non-alkaline conditions and are based on rare (and hence, expensive) elements, preventing their application on the massive scale required to replace fossil fuels. Third-row transition metals, such as Ni, Co, Fe and Mn, on the other hand, are much more abundant, and therefore, oxides of these elements are very attractive for the fabrication of anodic materials. The oxygen evolving complex in photosystem II, the catalyst used by green plants and some bacteria for oxidizing water, is indeed based on Earth-abundant elements, like Mn and Ca. It contains a Mn_4CaO_5 core with a distorted cubane structure [3], and recent experiments aimed at utilizing third-row elements within a similar cubane motif have achieved impressive results [4].

Molecular catalysts for water oxidation have also been intensively investigated [5], especially since the discovery of the "blue dimer" molecule (*cis*,*cis*-$[(bpy)^{2-}$ $(H_2O)Ru^{II}ORu^{II}(H_2O)(bpy)_2]^{4+}$) [6]. While in heterogeneous catalysts, it is usually difficult to identify the catalytically-active species, homogeneous catalysts are better suited to mechanistic studies [7]. Measuring the catalyst performance on a per-atom basis, molecular catalysts are in general more efficient than metal oxides, but they suffer from poor stability [8], since the organic ligands are quickly oxidized during the catalytic cycle.

Polyoxometalates (POMs) represent a special class of molecular catalysts, since they are fully-inorganic compounds that can serve as scaffolds to host different kinds of transition metal atoms or as ligands that stabilize multi-center metal-oxo cores. Recent experiments have shown that POMs with a metal-oxo core containing four transition metals atoms, like Ru [9,10], Co [11] or Mn [12], can be very

efficient water oxidation catalysts. There is an obvious structural analogy between the metal-oxo core of these molecules, containing four transition metal atoms, and the Mn_4CaO_5 core of the natural catalyst for water oxidation [3], also containing four transition metal centers.

The discovery that single-site catalysts can also be efficient catalysts for water oxidation [13] has led to significant progress in identifying the reaction mechanism, mostly due to the structural simplicity of their active site [14]. Single-site POMs have also been shown to be active in water oxidation, in particular a Ru-based POMs with the Keggin structure $[Ru^{III}(H_2O)XW_{11}O_{39}]^{5-}$ (X = Si, Ge) [15]. The mechanism of water oxidation promoted by this single-site catalysis has been proposed to involve a nucleophilic attack of a water molecule on a Ru-oxo intermediate [15,16], in line with with what we have recently proposed for the four-atom analog Ru_4-POM [17] and for a variety of Ru-based molecular catalysts [18].

It is suggested that both the single-site and multiple-site POMs can promote water oxidation with a common reaction mechanism and that they have a very similar local structural environment around the Ru site. In this work, we focus on the following fundamental questions: How does the water oxidation thermodynamics and overpotential depend on the number of active sites in these molecular catalysts? How does the reaction thermodynamics depend on the charge state of the metal centers? We provide insight into these fundamental issues by means of density functional theory (DFT) calculations. Our DFT simulations investigate the catalytic mechanism of water oxidation promoted by the single-site $[Ru^{III}(H_2O)SiW_{11}O_{39}]^{5-}$ (Ru-POM). The effects of the Ru oxidation state are investigated by studying analogous Ru-POM systems in which the Ru center has higher oxidation states, namely Ru(IV) and Ru(V). To assess the dependence of the reaction thermodynamics on the number of active sites in the molecular catalyst, we compare the results for the Ru-POM against those obtained for the Ru_4-POM $[Ru_4(\mu\text{-}O)_4(\mu\text{-}OH)_2(H_2O)_4)(\gamma\text{-}SiW_{10}O_{36})]^{10-}$ that we investigated in our previous works [17,19].

2. Computational Methods

2.1. Electronic Structure Calculations

The calculations are based on the spin-polarized DFT, and the exchange and correlation potential is approximated using either the Perdew–Burke–Ernzerhof (PBE) generalized gradient-corrected approximation [20] or the B3LYP hybrid functional [21,22]. This choice of exchange and correlation functionals is motivated by recent work [23] comparing the accuracy of DFT calculations using a variety of exchange and correlation functionals against highly accurate CCSD(T)calculations for water oxidation on a single-site Ru catalyst. This work has shown that hybrid functionals, such as B3LYP, PBE0 [24] and M06 [24], are the best-performing DFT methods, resulting in errors for the reaction energies and barriers for the rate-determining step of 1–2 kcal/mol. A similar conclusion was also recently drawn by computing the thermodynamics of water oxidation on Co-based catalysts [25].

The geometry optimizations of the single-center Ru-POM are performed with the LANL2DZbasis set, using the Los Alamos relativistic core potentials (EPCs) [26] for Ru and W atoms. The total energies are then computed with single-point (*i.e.*, fixed geometry) calculations using the Stuttgart–Dresden (SDD) basis set and EPC [27,28]. Solvation effects are included with the SMDsolvation model [29] through

single-point calculations on the optimized geometries. All of the above calculations were performed with the Gaussian 09 software [30].

The comparison of the thermodynamics for the single-center Ru-POM presented in this work with the results for the multiple-center Ru_4-POM catalysts described in our previous work [17,19] requires using the same level of theory for the two systems. The available energetics for water oxidation promoted by Ru_4-POM was obtained with the CP2Kcode [31]. To benchmark the reproducibility of the results when changing the code, we have therefore calculated the energetics of the catalytic cycle promoted by Ru-POM also with CP2K, employing the same computational parameters of [19]. This benchmark is reported in Appendix A. In the CP2K calculations, the Ru and W atoms are modeled using the DZVP-SR-MOLOPTbasis set, while for H and O atoms, we used the the TZV2P-MOLOPT basis set. The cutoff for the plane wave representation of the charge density was set to 350 Ry. The molecules were simulated in vacuum, in cubic boxes with a side of 24 Å, using the Martyna–Tuckerman method to decouple the periodic replicas of the system. More details regarding this computational approach can be found in our previous work [19].

To compute the effects of solvation in the Ru_4-POM molecule, we used the COSMO (conductor-like screening model) method [32], as implemented in the NWChemcode [33]. Due to the high computational cost of modeling this large molecule, solvation effects were in this case evaluated with a single-point calculation using the PBE functional and the TZVPbasis set. The solvation energy was then used to correct the B3LYP results obtained in a vacuum. Since the reactions we model in this work involve the addition and removal of hydrogen atoms from adsorbates in contact with the liquid environment, the notorious difficulty of implicit solvent models to describe hydrogen bonds accurately can lead to inaccuracies. However, the magnitude of these inaccuracies, as will be shown below, are significantly smaller than the magnitude of the reaction energies and the difference in reaction energies, which are the quantities of interest in this work.

2.2. The Water Oxidation Cycle

In this work, we investigate the energetics of the water oxidation reaction focusing on the free energy differences between the intermediates visited by the system along the reaction cycle. Following previous works [17,19], here, we assume that (i) all oxidation steps are coupled to a proton transfer, resulting in four consecutive proton-coupled electron-transfer (PCET) steps, and (ii) the O-O bond formation takes place through a nucleophilic attack of a solvent water molecule on a Ru-oxo species (also known as the acid-base mechanism). The water oxidation cycle investigated in this work is schematically shown in Figure 1. Several studies indicate this mechanism to be active on a variety of single- and multi-center molecular catalysts, including the well-known "blue dimer" [34] and the Ru_4-POM complex [17], and it has also been suggested to be at play in the case of metal oxide surfaces, such as RuO_2(110) [35].

Assuming we start with a metal center M in oxidation state n (M^n), the first step involves the removal of a proton from an incoming water and the oxidation of the metal center from oxidation state n to $n+1$ (M^{n+1}), leading to the formation of a hydroxo ligand. The second step involves the formation of an oxo intermediate and the formal oxidation of the metal to M^{n+2}. The following step consists of the nucleophilic attachment, resulting in a hydroperoxo ligand (OOH^-) and in the reduction of the metal

to M^{n+1}. The final step consists of the release of molecular oxygen and the reduction of metal back to the initial oxidation state (M^n). We stress that the oxidation states reported in Figure 1 are just formal oxidation states, while calculations show that, for example, in Ru(IV), the formation of the oxo ligand is accompanied by the reduction of the metal center and the formation of an oxyl ligand, leading to a Ru(V)-$O^{\cdot}$, rather than a Ru(VI)-O intermediate, as shown in our previous work [17]. Similarly, the OOH ligand has a radical character, reducing the Ru metal in a similar fashion to the oxyl radical.

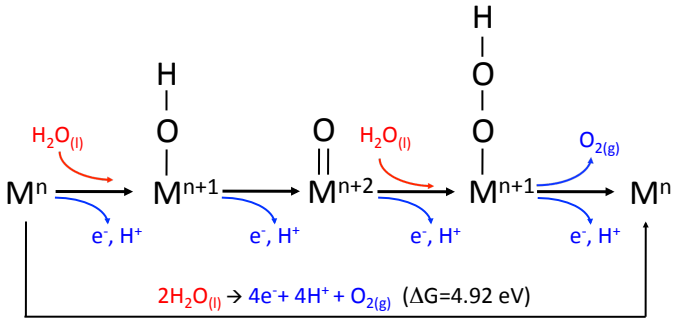

Figure 1. Scheme illustrating the water oxidation mechanism investigated in this work.

We note that the assumption that all oxidations are coupled to proton removal might not be valid under strongly acidic conditions. This is an important factor to consider in the comparison with the experiments. Indeed, Murakami *et al.* [15] showed that at low pH, the first oxidation does not involve a proton exchange, while the second one involves the loss of two protons.

2.3. Reaction Thermodynamics

The thermodynamics of the electrochemical catalytic cycle was studied with the protocol proposed by Nørskov *et al.* [36]. This approach allows for calculating the free energy difference among the various intermediates. Energy barriers between different reaction steps are not included in the approach. The method has been extensively applied to study water oxidation [35,37,38] and oxygen reduction [36] reactions on metal and metal oxide surfaces.

In this approach, all oxidations are assumed to be PCET steps. The advantage of this assumption is that the energetics of the electrochemical reaction can be referenced to the normal hydrogen electrode (NHE), and the problematic calculation of the distinct chemical potentials of H^+ and e^- can be avoided. By referring the calculated electrode potentials to the NHE, the free energy of the pair $H^+ + e^-$ is equal to half the free energy of a hydrogen molecule at standard conditions, which can be easily and accurately calculated:

$$H^+ + e^- \leftrightarrow 1/2H_2 \tag{3}$$

At zero bias and at pH $= 0$, the free energy change ΔG of a PCET step reaction is computed as:

$$\Delta G = \Delta E + \Delta ZPE + \Delta H - T\Delta S \tag{4}$$

where ΔE is the difference of the DFT total energies, ΔZPE is the change in zero point energy, computed using the DFT vibrational frequencies, and ΔH and ΔS are the changes in enthalpy and entropy, computed using standard thermodynamic tables [39].

The energy of the various reaction intermediates has been computed in standard conditions of temperature and pressure and pH = 0. The energy difference between the initial and final states corresponds to the free energy change of the reaction Equation (1), *i.e.*, 4.92 eV. Computing this number from first principles would involve the calculation of the O_2 molecule, which is known to be poorly described in DFT (especially using GGAfunctionals), and would result in a significant underestimation of the free energy cost to split water. We therefore use the experimental value and fix the last point of the oxidation cycle, corresponding to the release of $O_{2(g)}$ to be 4.92 eV higher than the initial point.

The effect of a finite bias U on a state involving one electron in the electrode is modeled by lowering the energy of this state by $-eU$. In this approach, the overpotential for the water oxidation reaction is simply defined as the potential at which all steps become downhill in energy. The effect of pH can be accounted for correcting the free energy of H^+ ions by the concentration dependence of the entropy, resulting in a term k_BT ln10 $\times$ pH to be added to the value of ΔG computed at pH = 0 [36,40].

3. Results and Discussion

3.1. Electronic Structure of Ru-POM: Dependency on the Ru Oxidation State

We start by characterizing the electronic structure of the [Ru(III)-POM]$^{5-}$ complex ([$Ru^{III}(H_2O)SiW_{11}O_{39}$]$^{5-}$) that consists of a Keggin-type polyoxometalate with a surface W atom substituted by a Ru atom. We show in Figure 2 the relaxed geometry obtained using the PBE functional.

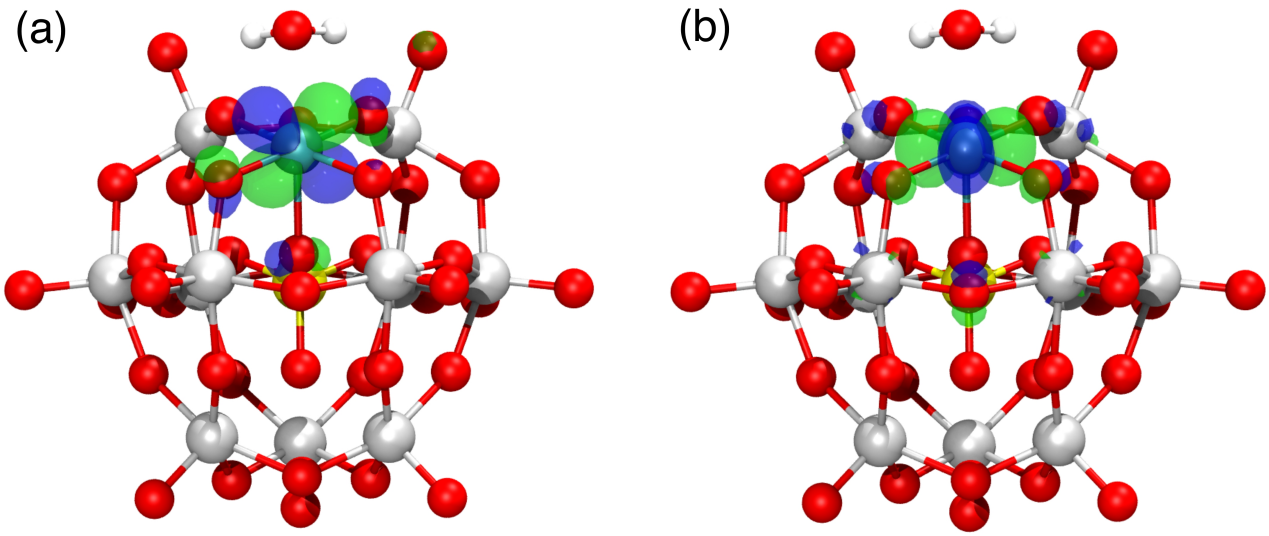

Figure 2. Relaxed geometry of the [Ru(III)-POM]$^{5-}$ molecule. Red, cyan, gray, yellow and white spheres represent O, Ru, W, Si and H atoms, respectively. The isosurface shows the spatial distribution of the HOMO (**a**) and LUMO (**b**) orbitals. POM, polyoxometalate.

The six-fold coordinated Ru ion is at the center of a distorted octahedron formed by five O ions of the POM molecule and by the O atom of the ligand water molecule. The octahedral ligand field induces a significant splitting of the t_{2g} and e_g levels. The charge and spin analysis of the ground state show that the Ru ion is in a low-spin d^5 electronic configuration, in which the five d electrons occupy the t_{2g} levels. This electronic configuration leaves one unpaired electron and, therefore, leads to a doublet state.

The highest occupied molecular orbital (HOMO) wavefunction is shown in Figure 2a: it is primarily localized on the Ru site and has a d_{xz} character. Similarly, we also find that the lowest unoccupied molecular orbital (LUMO) is mostly localized on the Ru ion (Figure 2b) and has a d_{xy} character. We find a HOMO-LUMO gap of 0.42 eV using the PBE functional and 2.85 eV using the B3LYP functional.

We now focus on the changes in the electronic structure resulting from oxidizing the [Ru(III)-POM]$^{5-}$ complex. In our computational setup, this can be achieved by reducing the number of electrons in the system, *i.e.*, by controlling the overall charge of the molecule.

The charge and spin analysis of the electronic ground states for the [Ru(IV)-POM]$^{4-}$ and [Ru(V)-POM]$^{3-}$ systems are reported in Table 1. The values of the Mulliken spin polarization at the Ru site were obtained with both the PBE and B3LYP functional. In each case, we report only the values corresponding to the lowest-energy spin configuration. The calculated Mulliken spin polarization follows the trend expected when going from a doublet in the case of Ru(III) to a triplet for Ru(IV) and to a doublet for Ru(V). In the case of a doublet, a single unpaired spin should result in μ equal to 1.0, while a triplet should result in μ equal to 2.0. We find lower values, indicating a certain degree of delocalization of the Mulliken spin density outside the Ru ion. We also find, in agreement with previous calculations [19], that hybrid functionals lead to a slightly larger localization of the spin density at the metal site, compared to the semi-local GGA-type of functionals.

Table 1. Mulliken spin polarization at the Ru ion as a function of the Ru oxidation state, evaluated in a vacuum. OS indicates the oxidation state of the Ru ion, "conf." the electronic configuration, Q the total charge of the anion, 2S + 1 the multiplicity and μ the Mulliken spin polarization in Bohr magnetons at the Ru ion obtained with the two functionals. PBE, Perdew–Burke–Ernzerhof.

OS	Conf.	Q	2S + 1	μ(PBE)	μ(B3LYP)
Ru(III)	d^5	−5	2	0.74	0.81
Ru(IV)	d^4	−4	3	1.31	1.48
Ru(V)	d^3	−3	2	0.76	0.67

3.2. Thermodynamics of the Water Oxidation Cycle

3.2.1. Ru-POM and the Effect of Ru Oxidation State

In Figure 3, we show the free energy cost to oxidize water along the reaction steps of the mechanism displayed in Figure 1. The reaction energetics is reported for the Ru-POM catalyst in both vacuum conditions (open symbols) and in solution (filled symbols and solid lines). Different colors of lines and symbols denote different charge states of the catalyst. The actual values of the free energy steps are also reported in Table 2.

The catalytic cycle promoted by Ru(III)-POM is denoted by the black symbols. The calculated energetics show that, when considering solvation effects, the step requiring the largest free-energy difference (2.06 eV) is determined by the formation of the hydroperoxo intermediate *OOH. The figure shows the free energy change along the oxidation cycle also for the Ru(IV)-POM and Ru(V)-POM

catalysts. By increasing the oxidation state of the Ru atom, the free energy cost of the formation of hydroperoxo intermediate reduces while the cost for the second oxidation, the formation of the oxo intermediate, increases. In fact, we can see that the cost of those two steps is very similar for the Ru(IV)-POM catalyst (1.73 eV and 1.78 eV), while in the case of Ru(V)-POM, the formation of the *O intermediate becomes the most demanding step (1.83 eV).

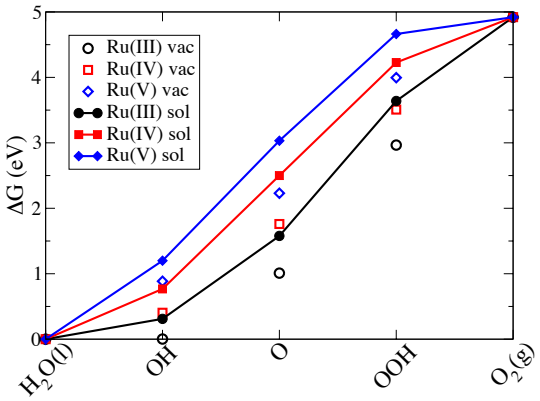

Figure 3. B3LYP free energy changes along the reaction cycle for single-center Ru-POMs with the Ru atom in different oxidation states (III, IV and V). Filled symbols represent the calculations performed accounting for the solvation effects, while empty symbols the calculations perfumed in a vacuum.

Table 2. Free energy changes along the catalytic cycle for the single-center Ru-POM and for Ru_4(IV)-POM computed with the B3LYP functional. Both results in a vacuum and in solution are reported.

Intermediate	**In Vacuum**				**In Solution**			
	Ru(III)	**Ru(IV)**	**Ru(V)**	**Ru_4(IV)**	**Ru(III)**	**Ru(IV)**	**Ru(V)**	**Ru_4(IV)**
H_2O(l)	0.00	0.00	0.00	0.00	0.00	0.00	0.00	0.00
*OH	0.00	0.40	0.89	0.78	0.31	0.77	1.20	0.72
*O	1.01	1.76	2.23	2.50	1.58	2.50	3.03	2.65
*OOH	2.97	3.01	4.00	4.20	3.64	4.28	4.66	4.35
O_2(g)	4.92	4.92	4.92	4.92	4.92	4.92	4.92	4.92

We can understand these results using the fact that the sum of the free energy cost to perform the second and third oxidation, *i.e.*, the transformation of a hydroxo ligand into a hydroperoxo ligand, is a universal constant independent of the catalyst. According to these results of Man *et al.* [41], the sum of these two steps has a free energy cost of 3.2 ($\pm$0.2 eV, 67% confidence interval, and $\pm$0.4 eV, 95% confidence interval), and in fact, we find values of 3.33, 3.51 and 3.46 eV for Ru(III)-, Ru(IV)- and Ru(V)-POM, respectively. The increase of the oxidation state of Ru leads to weaker bonding of the *O intermediate, and as a result, the free energy cost to form *OOH from *O decreases while the free energy cost to form *O from *OH increases. This is consistent with the fact that for Ru(III), where

the *O binding energy is stronger (1.44 eV, where larger numbers indicate weaker binding), the most demanding step is the formation of *OOH, while for Ru(V), where the *O binding energy is weaker (2.90 eV), the most demanding step is the formation of *O. Ru(IV) offers the best compromise, with a *O binding energy of 2.36 eV, leading to the free energy cost to form *O and *OOH being very similar.

According to the protocol proposed by Nørskov *et al.* [36], the overpotential for Ru(III)-POM is equal to 2.06 − 1.23 = 0.83 V, while we obtain 0.55 V and 0.60 V for Ru(IV)- and Ru(V)-POM. An important result of our investigation is therefore that the best single-center Ru-POM catalyst with a Keggin structure is the one containing a Ru(IV) ion. Since the free energy cost of the two most demanding steps is very close (within 0.05 eV), this catalyst is almost optimal, within the constraint highlighted by Man *et al.* [41]. A similar conclusion was also reached in our previous work on the four-center Ru_4(IV)-POM [17].

3.2.2. Ru-POM *vs.* Ru_4-POM: The Effect of the Number of Ru Centers

In Figure 4a, we compare the energetics of the water oxidation cycle promoted by Ru-POM, considering Ru(III), Ru(IV) and Ru(V) single centers, with the one promoted by the four-center $Ru(IV)_4$-POM. In all cases, the calculations are performed using the B3LYP functional and accounting for solvation effects, as described in the Methodssection. The striking result of this comparison is that the values obtained for $Ru(IV)_4$-POM nicely match those for the single-center Ru(IV)-POM. This suggests that the most important factor in determining the energy cost of the four steps of the water oxidation cycle is the oxidation state of the metal center promoting the reaction, regardless of the number of metal centers. We stress here that the local atomistic environment around the Ru center, namely the octahedron formed by the six oxygen atoms neighboring the metal center, is similar in the single-site and multiple-site molecular catalysts.

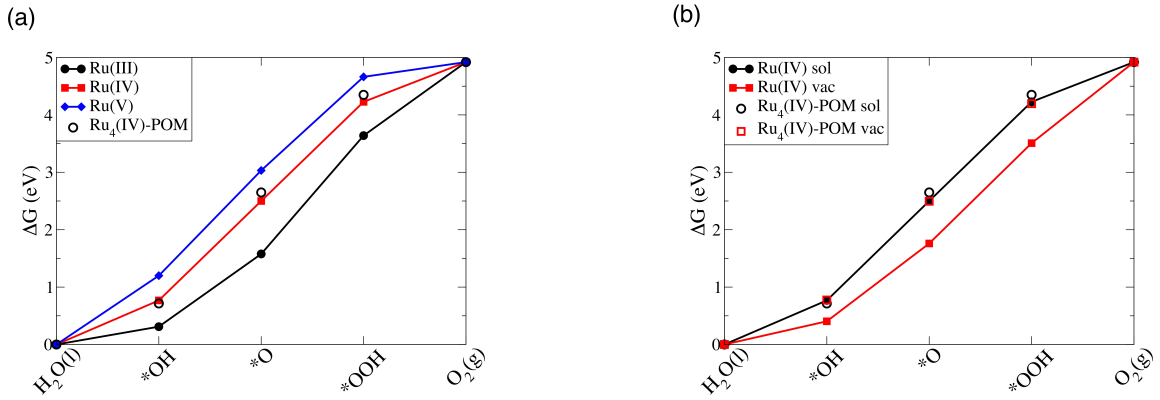

Figure 4. (**a**) B3LYP free energy changes along the reaction cycle computed in solution; (**b**) comparison of the effect of solvation on Ru(IV)-Keggin and $Ru(IV)_4$-POM.

Our results show that the molecular structure beyond the first O shell of the Ru active site has minor effects on the catalyst overpotential, which is instead primarily governed by the oxidation state of the metal site.

In addition, Figure 4b shows that solvation effects are much larger in the single-center Ru(IV)-POM compared to the four-center Ru_4(IV)-POM. This implies that the agreement discussed above is found

only in solution, not in a vacuum. The reason for this behavior is likely due to electrostatic effects originating from the large charge of the the anions (-4 for Ru-POM and -10 for Ru_4(IV)-POM), which obviously cannot be screened when the calculations are performed in a vacuum. These effects manifest more clearly in the smaller catalyst, while is negligibly small for the larger Ru_4(IV)-POM, as already argued in our previous work [19].

4. Conclusions

In summary, we have used DFT calculations to investigate the water oxidation reaction catalyzed by single-center Ru-based polyoxometalates with the Keggin structure. By controlling the overall charge of the molecule, we were able to study the energetics of the reaction cycle as a function of the oxidation state of the Ru center. We found that the Ru(IV) ion leads to a lower overpotential compared to Ru(III) and Ru(V), which we rationalized on the basis of the strength of the Ru-Ointeraction. When compared against the Ru_4(IV)-POM catalyst, we found that the single-center and the multi-center catalysts based on the Ru(IV) ion display very similar energetics. For reaction mechanisms based on a single site, our results show that the electronic structure of the active metal ion controls the energy cost of the oxidation steps, while the local structure around the Ru sites beyond the first O shell does not contribute appreciably. Solvent effects are remarkably important for the smaller Keggin-type single-center molecules, while the Ru_4(IV)-POM molecule, likely due to its much larger size, is able to effectively screen its charge and, hence, display smaller effects of the solvent on its catalytic properties.

Acknowledgments

We acknowledge computational time on the Hermit supercomputer at HRLS, Germany, through the PRACEproject "ENCORASOL—Engineering multi-core transition metal catalysts for solar fuel production" and at CINECAHPCcenter, Italy. This work was partially supported by the EU FP7 COST action CM104and by the FP7-NMP-2012 project chipCAT

under Contract No. 310191. We are grateful to Andrea Sartorel and Marcella Bonchio for useful discussions.

Author Contributions

S.P. performed the calculations and the analysis. S.P. and S.F. planned the project and wrote the manuscript.

Conflicts of Interest

The authors declare no conflict of interest.

Appendix

A. Estimating the Error Bar in the Computed Thermodynamics

In this work, we employ different computational approaches to estimate the dependency of the reaction thermodynamics on the number and oxidation state of the active centers. This is necessary because the present data for the Ru-POM system are obtained with the Gaussian 09 code, while the available results for the Ru_4-POM system were obtained with the the CP2K code [17,19]. It is therefore useful to assess the error bar of this analysis by comparing the results obtained with the two approaches for the same system, namely the water oxidation cycle promoted by the single-center Ru(III)-POM in a vacuum.

In both cases, we use the B3LYP functional, while the choice of basis sets and pseudopotentials differ: in the case of CP2K calculations, we use DZVP-MOLOPT for Ru and W, TZVP-MOLOPT for O and H and GHTpseudopotentials [42], while in the case of Gaussian 09 calculations, we use SDD basis sets and effective core potentials. In both cases, the structures are optimized using the default thresholds on forces. In Table A1, we compare the free energy changes along the catalytic cycle obtained using the two approaches. The differences are in all cases small, the largest one being equal to 0.16 eV in the second step. While this difference is not negligible, indicating that our calculations are likely not fully converged with respect to the basis set, it is small enough to allow meaningful comparisons between the results obtained in our previous work on the four-center Ru_4-POM and the single-center Ru-POM.

Table A1. Comparison of the free energy changes along the catalytic cycle computed using CP2K(B3LYP/DZVP-TZV2P) and Gaussian (B3LYP/SDD-TZVP). Both sets of calculations are performed in a vacuum.

Intermediate	CP2K	Gaussian
H_2O(l)	0.00	0.00
*OH	−0.05	0.00
*O	1.17	1.01
*OOH	2.98	2.97
O_2(g)	4.92	4.92

One more source of error in our approach, when comparing solvation effects in Ru-POM and Ru_4-POM, is the use of two different solvation models, SMD and COSMO. We therefore evaluated the discrepancy between the two models on the smaller Ru(III)-POM molecule, for the case of a H_2O ligand. The SMD differences with respect to the vacuum case (*i.e.*, the solvation effects) in the free energy costs of the first three steps (the fourth step is set to 4.92 eV by construction) are 0.31 eV, 0.57 eV and 0.67 eV, respectively. The values obtained with the COSMO solvation model are 0.17 eV, 0.29 eV and 0.44 eV. The differences between the two solvation models are of the order of 0.2 eV, with the COSMO model resulting in smaller solvation effects. Furthermore, in this case, therefore, the errors are sufficiently small to allow for a meaningful comparison of the results obtained with these two different solvation models.

References

1. Lewis, N.S.; Nocera, D.G. Powering the planet: Chemical challenges in solar energy utilization. *Proc. Natl. Acad. Sci. USA* **2006**, *103*, 15729–15735.
2. Balzani, V.; Credi, A.; Venturi, M. Photochemical conversion of solar energy. *ChemSusChem* **2008**, *1*, 26–58.
3. Suga, M.; Akita, F.; Hirata, K.; Ueno, G.; Murakami, H.; Nakajima, Y.; Shimizu, T.; Yamashita, K.; Yamamoto, M.; Ago, H.; *et al.* Native structure of photosystem II at 1.95 A resolution viewed by femtosecond X-ray pulses. *Nature* **2015**, *517*, 99–103.
4. Kanan, M.W.; Nocera, D.G. *In situ* formation of an oxygen-evolving catalyst in neutral water containing phosphate and Co^{2+}. *Science* **2008**, *321*, 1072–1075.
5. Karkas, M.D.; Verho, O.; Johnston, E.V.; Pkermark, B. Artificial Photosynthesis: Molecular Systems for Catalytic Water Oxidation. *Chem. Rev.* **2014**, *114*, 11863–12001.
6. Gersten, S.W.; Samuels, G.J.; Meyer, T.J. Catalytic oxidation of water by an oxo-bridged ruthenium dimer. *J. Am. Chem. Soc.* **1982**, *104*, 4029–4030.
7. Dau, H.; Limberg, C.; Reier, T.; Risch, M.; Roggan, S.; Strasser, P. The Mechanism of Water Oxidation: From Electrolysis via Homogeneous to Biological Catalysis. *ChemCatChem* **2010**, *2*, 724–761.
8. Limburg, B.; Bouwman, E.; Bonnet, S. Molecular water oxidation catalysts based on transition metals and their decomposition pathways. *Coord. Chem. Rev.* **2012**, *256*, 1451–1467.
9. Sartorel, A.; Carraro, M.; Scorrano, G.; Zorzi, R.D.; Geremia, S.; McDaniel, N.; Bernhard, S.; Bonchio, M. Polyoxometalate embedding of a tetraruthenium(IV)-oxo-core by template-directed metalation of $[\gamma\text{-}SiW_{10}O_{36}]^{8-}$: a totally inorganic oxygen-evolving catalyst. *J. Am. Chem. Soc.* **2008**, *130*, 5006–5007.
10. Geletii, Y.V.; Botar, B.; Kögerler, P.; Hillesheim, D.A.; Musaev, D.G.; Hill, C.G. An all-inorganic, stable, and highly active tetraruthenium homogeneous catalyst for water oxidation. *Agew. Chem. Int. Ed.* **2008**, *47*, 3896–3899.
11. Yin, Q.; Tan, J.M.; Besson, C.; Geletii, Y.V.; Musaev, D.G.; Kuznetsov, A.E.; Luo, Z.; Hardcastle, K.I.; Hill, C.L. A Fast Soluble Carbon-Free Molecular Water Oxidation Catalyst Based on Abundant Metals. *Science* **2010**, *328*, 342–345.
12. Al-Oweini, R.; Sartorel, A.; Bassil, B.S.; Natali, M.; Berardi, S.; Scandola, F.; Kortz, U.; Bonchio, M. Photocatalytic Water Oxidation by a Mixed-Valent MnIII3MnIVO3 Manganese Oxo Core that Mimics the Natural Oxygen-Evolving Center. *Agew. Chem. Int. Ed.* **2014**, *53*, 11182–11185.
13. McDaniel, N.D.; Coughlin, F.J.; Tinker, L.L.; Bernhard, S. Cyclometalated iridium(III) Aquo complexes: efficient and tunable catalysts for the homogeneous oxidation of water. *J. Am. Chem. Soc.* **2008**, *130*, 210–217.
14. Wasylenko, D.J.; Palmer, R.D.; Berlinguette, C.P. Homogeneous water oxidation catalysts containing a single metal site. *Chem. Commun.* **2013**, *49*, 218–227.

15. Murakami, M.; Hong, D.; Suenobu, T.; Yamaguchi, S.; Ogura, T.; Fukuzumi, S. Catalytic mechanism of water oxidation with single-site ruthenium-heteropolytungstate complexes. *J. Am. Chem. Soc.* **2011**, *133*, 11605–11613.
16. Lang, Z.L.; Yang, G.C.; Ma, N.N.; Wen, S.Z.; Yan, L.K.; Guan, W.; Su, Z.M. DFT characterization on the mechanism of water splitting catalyzed by single-Ru-substituted polyoxometalates. *Dalton Trans.* **2013**, *42*, 10617–10625.
17. Piccinin, S.; Sartorel, A.; Bonchio, M.; Fabris, S. Water oxidation surface mechanisms replicated by a totally inorganic tetraruthenium-oxo molecular complex. *Proc. Natl. Acad. Sci. USA* **2013**, *110*, 4917–4922.
18. Romain, S.; Vigara, L.; Llobet, A. Oxygen-Oxygen Bond Formation Pathways Promoted by Ruthenium Complexes. *Acc. Chem. Res.* **2009**, *42*, 1944–1953.
19. Piccinin, S.; Fabris, S. First principles study of water oxidation catalyzed by a tetraruthenium-oxo core embedded in polyoxometalate ligands. *Phys. Chem. Chem. Phys.* **2011**, *13*, 7666–7674.
20. Perdew, J.P.; Burke, K.; Ernzerhof, M. Generalized Gradient Approximation Made Simple. *Phys. Rev. Lett.* **1996**, *77*, 3865.
21. Becke, A.D. Densityfunctional thermochemistry. III. The role of exact exchange. *J. Chem. Phys.* **1993**, *98*, 5648.
22. Stephens, P.; Devlin, F.J.; Chabalowski, C.F.; Frisch, M.J. Ab Initio Calculation of Vibrational Absorption and Circular Dichroism Spectra Using Density Functional Force Fields. *J. Phys. Chem.* **1994**, *98*, 11623.
23. Kang, R.; Yao, J.; Chen, H. Are DFT Methods Accurate in Mononuclear Ruthenium-Catalyzed Water Oxidation? An ab Initio Assessment. *J. Chem. Theory Comput.* **2013**, *9*, 1872–1879.
24. Perdew, J.P.; Burke, K.; Ernzerhof, M. Rationale for mixing exact exchange with density functional approximations. *J. Chem. Phys.* **1996**, *105*, 9982.
25. Kwapien, K.; Piccinin, S.; Fabris, S. Energetics of Water Oxidation Catalyzed by Cobalt Oxide Nanoparticles: Assessing the Accuracy of DFT and DFT+U Approaches against Coupled Cluster Methods. *J. Phys. Chem. Lett.* **2013**, *4*, 4223–4230.
26. Hay, P.J.; Wadt, W.R. Ab initio effective core potentials for molecular calculations. Potentials for the transition metal atoms Sc to Hg. *J. Chem. Phys.* **1985**, *82*, 270.
27. Andrae, D.; Haussermann, U.; Dolg, M.; Stoll, H.; Preuss, H. Energy-adjusted ab initio pseudopotentials for the second and third row transition elements. *Theor. Chem. Acc.* **1990**, *77*, 123–141.
28. Dolg, M.; Wedig, U.; Stoll, H.; Preuss, H. Energy-adjusted ab initio pseudopotentials for the first row transition elements. *J. Chem. Phys* **1987**, *86*, 866.
29. Marenich, A.V.; Cramer, C.J.; Truhlar, D.G. Universal Solvation Model Based on Solute Electron Density and on a Continuum Model of the Solvent Defined by the Bulk Dielectric Constant and Atomic Surface Tensions. *J. Phys. Chem. B* **2009**, *113*, 6378–6396.
30. Frisch, M.J.; Trucks, G.W.; Schlegel, H.B.; Scuseria, G.E.; Robb, M.A.; Cheeseman, J.R.; Scalmani, G.; Barone, V.; Mennucci, B.; Petersson, G.A.; *et al.* *Gaussian 09 Revision D.01*; Gaussian Inc.: Wallingford, CT, USA, 2009.

31. VandeVondele, J.; Krack, M.; Mohamed, F.; Parrinello, M.; Chassaing, T.; Hutter, J. Fast and accurate density functional calculations using a mixed Gaussian and plane waves approach. *Comp. Phys. Comm.* **2005**, *167*, 103–128.
32. Klamt, A.; Schuurmann, G. COSMO: a new approach to dielectric screening in solvents with explicit expressions for the screening energy and its gradient. *J. Chem. Soc. Perkin Trans. 2* **1993**, 799–805.
33. Valiev, M.; Bylaska, E.; Govind, N.; Kowalski, K.; Straatsma, T.; Dam, H.V.; Wang, D.; Nieplocha, J.; Apra, E.; Windus, T.; *et al*. NWChem: A comprehensive and scalable open-source solution for large scale molecular simulations. *Comp. Phys. Comm.* **2010**, *181*, 1477 – 1489.
34. Liu, F.; Concepcion, J.J.; Jurss, J.W.; Cardolaccia, T.; Templeton, J.L.; Meyer, T.J. Mechanisms of water oxidation from the blue dimer to photosystem II. *Inorg. Chem.* **2008**, *47*, 1727–1752.
35. Rossmeisl, J.; Qu, Z.W.; Zhu, H.; Kroes, G.J.; Nørskov, J.K. Electrolysis of water on oxide surfaces. *J. Electroanal. Chem.* **2007**, *607*, 83–89.
36. Nørskov, J.K.; Rossmeisl, J.; Logadottir, A.; Lindqvist, L.; Kitchin, J.R.; Bligaard, T.; Jonsson, H. Origin of the Overpotential for Oxygen Reduction at a Fuel-Cell Cathode. *J. Phys. Chem. B.* **2004**, *108*, 17886–17892.
37. Rossmeisl, J.; Logadottir, A.; Nørskov, J.K. Electrolysis of water on (oxidized) metal surfaces. *Chem. Phys.* **2005**, *319*, 178–184.
38. Rossmeisl, J.; Nørskov, J.K.; Taylor, C.D.; Janik, M.J.; Neurock, M. Calculated phase diagrams for the electrochemical oxidation and reduction of water over Pt(111). *J. Phys. Chem. B* **2006**, *110*, 21833–21839.
39. Stull, D.; Prophet, H. *JANAF Thermochemical Tables*, 2nd ed.; U.S. National Bureau of Standards: Washington, DC, USA, 1971.
40. Cheng, J.; Liu, X.; Kattirtzi, J.A.; VandeVondele, J.; Sprik, M. Aligning Electronic and Protonic Energy Levels of Proton-Coupled Electron Transfer in Water Oxidation on Aqueous TiO_2. *Angew. Chem.* **2014**, *126*, 12242–12246.
41. Man, I.C.; Su, H.Y.; Calle-Vallejo, F.; Hansen, H.A.; Martinez, J.I.; Inoglu, N.G.; Kitchin, J.; Jaramillo, T.F.; Norskov, J.K.; Rossmeisl, J. Universality in Oxygen Evolution Electrocatalysis on Oxide Surfaces. *ChemCatChem* **2011**, *3*, 1159–1165.
42. Goedecker, S.; Teter, M.; Hutter, J. Separable dual-space Gaussian pseudopotentials. *Phys. Rev. B* **1996**, *54*, 1703–1710.

© 2015 by the authors; licensee MDPI, Basel, Switzerland. This article is an open access article distributed under the terms and conditions of the Creative Commons Attribution license (http://creativecommons.org/licenses/by/4.0/).